The energetics of 'airtime': estimating swim power from breaching behaviour in fishes and cetaceans

Lewis G. Halsey[1] and Gil Iosilevskii[2]

[1]University of Roehampton, London SW15 4JD, UK
[2]Technion, Haifa 32000, Israel

Author for correspondence: Lewis G. Halsey, l.halsey@roehampton.ac.uk

Abstract

Maximum swimming behaviour is rare in the laboratory or the wild, limiting our understanding of the top-end athletic capacities of aquatic vertebrates. However, jumps out of the water - exhibited by a diversity of fish and cetaceans - might sometimes represent a behaviour of maximum burst effort. We collected data on such breaching behaviour for 14 fish and cetacean species primarily from online videos, to calculate breaching speed. From newly derived formulae based on the drag coefficient and hydrodynamic efficiency we also calculated the associated power. The fastest breaching speeds were exhibited by species 2 m in length, peaking at nearly 11 m/s; from this length, as species size decreases the fastest breaches become slower, while species larger than 2 m do not show a systematic pattern. The power associated with the fastest breaches was consistently about 50 W/kg (equivalent to 200 W/kg muscle) in species from 20 cm to 2 m in length; this value may represent a universal (conservative) upper boundary. And it is similar to the maximum recorded power output per muscle mass recorded in any species of similar size, suggesting that some breaches could indeed be representative of maximum capability.

Introduction

The maximum speeds an animal can achieve are rarely displayed in the laboratory, or indeed in the field; wild animals are only occasionally observed moving flat out (Lutcavage et al., 2000; Wilson et al., 2015). Even during predator-prey interactions, maximum speeds are rarely exhibited (e.g. Husak et al., 2006). Measures of maximum power in animals are therefore difficult to obtain, and methods that encourage maximum physical effort from subject animals can be ethically questionable. This is unfortunate, because an understanding of maximum speed and power provides insights into the morphological and physiological capabilities and limitations that have evolved in species usually highly adapted to the environments they inhabit.

Possibly, however, there is a natural behaviour exhibited by a diversity of aquatic animals that is not only sometimes undertaken with maximum speed and power but is also easy to record – jumping clear of the water, otherwise known as breaching. In some species at least, locomotion speed is documented to be greater during breaching than at any other time (Johnston et al., 2018; Watanabe et al., 2013). There is only a small amount of published data quantifying the nature of breaches in jumping animals (Tanaka et al., 2019), but many breaches have been documented on video, which are freely available on the world wide web. An initial estimate of an animal's breaching speed can often be obtained from video recordings simply

by timing the duration that the animal is above the water surface, coupled with breaching angle from horizontal (Johnston et al., 2018). From breaching speed, the mechanical power needed to achieve that speed can be estimated with knowledge of the drag coefficient and hydrodynamic efficiency. In turn, the drag coefficient can be estimated using semi-empirical methods (Iosilevskii and Papastamatiou, 2016); the hydrodynamic propulsion efficiency (the ratio of the mechanical power to the power supplied by the muscles) can be estimated from swimming gait. We present and interpret the analysis of the speed and power of breaching by fish and cetaceans ranging in length from 20 cm to 14 m.

Methods

Data on breaching speed and breaching angle from horizontal were collected for 14 species of fishes and cetaceans spanning (tip of snout to fork of tail) lengths from 0.2 to 14 m (Table 1). Breaching data were obtained predominantly from videos available on www.youtube.com. Only those segments of video that represented the entirety of clearly discernible jumps shown at full speed were analysed. The time that the animal was out of the water τ during a breach was estimated from video footage, following a refined approach to that taken by Johnston et al. (2018) for basking and white sharks; that study also validated the approach with direct measures of speed obtained from an animal-attached data logger. The time was measured from the moment the snout of the animal broke the water surface until the animal's estimated centre of mass reached the same height above the water on descent that it was during ascent at the point that the body just cleared the water. The angle of the breach from horizontal, γ, was estimated visually at the same point (only breaches close to vertical were included in analysis). Justification of this approach is in Supplementary Appendix A. The length of the animal was bracketed +/- 30% around the typical length associated with the particular species based on direct observations where possible (Parsons et al., 2016), or otherwise specialist taxonomy websites, Wikipedia and FishBase.

The speed of the animal just prior to piercing the water surface, v_0, was estimated from the time it spent out of the water τ with

$$v_0 \approx \frac{g\tau}{2\sin\gamma}\left(1 - \frac{A}{4}\right) - \frac{l}{\tau}\cos^2\gamma,$$

(1)

where g is the acceleration of gravity, l is body length, γ is the angle of the breach from horizontal, and A is the ratio of the drag coefficient based on the maximal area of the animal in the traverse plane and prismatic coefficient of its body (the ratio between the volume of the

body and the minimal cylinder enclosing it). The derivation of (1) is in Supplementary Appendix A. In equation (1), the first factor $\dfrac{g\tau}{2\sin\gamma}$ is the breach velocity that the animal would have had if it were a point mass; the second factor $(1-A/4)$ is the correction due to the animal accelerating when piercing the water surface (even if it had reached a constant velocity beforehand) owing to differences in drag between moving in water and air; the last term, $\dfrac{l}{\tau}\cos^2\gamma$, corrects for the change in trajectory angle during the breach (the breaching angle is set when the animal clears the water). When breaching at angles close to vertical, the last term becomes negligibly small

The key assumptions underlying equation (1) are:

a. the animal is neutrally buoyant,

b. it has a fusiform body resembling a double ogive,

c. its fins are retracted,

d. it reaches a constant velocity v_0 prior to piercing the water surface,

e. it continues to supply constant thrust until its tail leaves the water.

Fortuitously, under assumptions (b) and (c), when the body has width-to-length ratio between 0.15 and 0.25, A can be closely approximated by

$$A \approx (35/2)\,C_f\left(\mathrm{Re}_l\right), \tag{2}$$

where

$$C_f \approx 0.455 \big/ \mathrm{Re}_i^{2.58} \tag{3}$$

is the effective (turbulent) friction coefficient between the animal skin and water, which depends solely on the Reynolds number $\mathrm{Re}_l = v_0 l/\nu$ (ν being the kinematic viscosity of water) – details can be found in Supplementary Appendix B. When some of the fins are either non-retractable or being purposely extended, the combination of (2) and (3) furnishes the lower bound of A. It also underestimates the true value of A at high Reynolds numbers, where the thickness of the boundary layer on the animal becomes comparable with the height of the roughness elements on its skin. Thus it is possible that we overestimate the true breaching speed. Nonetheless, because a typical value of A is 0.1 (Table 1), even if the error in A is 30%, the resulting error in v_0 remains small (see Supplementary Appendix C). In fact, under most circumstances, a point mass approximation of v_0,

$$v_0 \approx \frac{g\tau}{2\sin\gamma},\tag{4}$$

will be fairly accurate (and was the approximation used in Johnston et al. 2018). Assumption (d) can be investigated in the two species which to date have been measured breaching via an animal-attached data logger – basking sharks and white sharks. In both cases the data suggest that the breaching animals were not accelerating by the time their snouts had reached the water surface (Johnston et al., 2018; Semmens et al., 2019; Semmens pers. comm.)

Mechanical power per unit mass (P/m) that the animal needs to swim at velocity v_0 was estimated with

$$\frac{P}{m} = \frac{A}{\eta_h} \frac{v_0^3}{l},\tag{5}$$

where η_h is the hydrodynamic propulsion efficiency – details can be found in Supplementary Appendix B. We have set $\eta_h = 0.9$ at the upper (theoretical) limit of propulsion efficiency of carangiform and thunniform gaits (Chopra and Kambe, 1977; Liu and Bose, 1997). Again, because of our underestimating the true value of A and the application of purposefully high values of propulsions efficiency, the value furnished by the combination of equations (2) to (5) should be considered the lower bound for all species that cleared the water when breaching, in spite of a possible error in v_0 (see Supplementary Appendix C). For large species that did not leave the water completely, equations (1) and (5) may overestimate both their speed and power, but bearing this in mind will strengthen the interpretations of the data presented in the Discussion section.

Estimation errors in equations (1) and (5) are assessed in Supplementary Appendix C. To minimize these errors, only high jumps (where γ exceeded 70 degrees) were included. Under this restriction, the errors in the breaching speed v_0 are estimated at about 10%, whereas the errors in the mass-specific power (P/m) can possibly reach 30%.

Results and Discussion

Velocities of all breaches for each species for which the breaching angle exceeded 70 degrees, and the mass-specific mechanical power deemed needed to achieve these, are plotted against body length in Fig. 1. Maximum breaching speed has an upper bound of about 11 m/s, while maximum mass-specific power has an upper bound of about 50 W/kg. These limits coincide at about 2-m body length. Breaching velocity increases up to 2-m body length with larger animals

not exhibiting a systematic relationship between length and velocity; mass-specific power is approximately constant up to 2-m body length, at around 50 W/kg, and is variously lower at greater body sizes. While sample size varies considerably between species, there is no substantive regression between the mean breaching speed of the top three fastest breaches and sample size (Spearman's rho: 0.141; p = 0.645). The breaching velocity of common bottlenose dolphins has been determined by an alternate method, high speed underwater camera (Rohr et al., 2002), which returned a range of maximum speeds similar to those we report, providing further validation for our method.

Based on our calculations, as species get larger up to 2 m in length, maximum breaching velocity exhibited increases, to a highest breaching velocity of nearly 11 m/s (achieved by the common bottlenose dolphin; Figure 1A).

There is some suggestion from the breaching data that a number of particularly large animals do not exhibit higher breaching speeds than do 2-m long species. The maximum swimming speed of an animal is limited either by its maximal thrust or its maximal power (Iosilevskii and Papastamatiou, 2016). Thus maximum swimming speed is the lower of the theoretical speeds at which hydrodynamic drag equals maximal thrust, and at which rate of work done by the animal on the water (loosely, the product of drag and speed) equals maximal power. Maximal thrust is proportional to the cross section area of the animal's locomotion muscles, and hence scales with the length of the animal squared. Maximal power is proportional to the volume (mass) of those muscles, and hence scales with the length of the animal to the third power. Because hydrodynamic drag is proportional to the product of the swimming speed squared and length of the animal squared, while maximal thrust is proportional to animal length squared, if the maximal speed is limited by muscle thrust, maximal speed should be independent of length. If, on the other hand, the maximal speed of an animal is limited by power, it should scale with length to the power (1/3). Our data suggests that for animals smaller than 2 m in length, the breaching speed increases with length to the power (1/3), implying that it is limited by the mass-specific (volume-specific) power of the locomotion muscles. For larger animals, the breaching speed remains practically independent of length, implying that it is limited by the alternative possibility – the thrust it can generate per unit cross section area of its muscles.

Figure 1A also includes data for burst swimming fish during containment in several different swimming apparatuses reported across multiple studies (taken from Table 4 in Videler et al. 1991). In all cases except for small mackerel, the maximum speeds observed in the lab

for burst swimming fish are much lower than breaching speeds we calculated for similarly sized species, suggesting that those burst swimming fish were swimming sub-maximally. Castro-Santos et al. (2012) have developed a flume larger than used in previous studies of fast swimming fish, which appears to elicit close to maximal swimming speeds in multiple relatively small species. Trout *Salvelinus fontinalis* and *Salmo trutta* of 0.145-m length volitionally swum against a fixed flow at up to about 4 m/s, while herring *Alosa aestivalis* (0.22 m) reached 4.5 m/s. Similar feats were observed in comparably sized barbels *Luciobarbus comizo* and nase *Pseudochondrostoma duriense* (Sanz-Ronda et al., 2015). These speeds are remarkably similar to the highest speeds we would predict species of this size would breach at based on our data (Figure 1A). Due to size constraints, however, very few fish greater than 1 m in length have been swum in the laboratory (though see Sepulveda et al., 2007), particularly at higher speeds.

Small cetaceans can be trained to swim fast in captivity, and the fastest swimming speed reported for dolphins under such conditions (11 m/s; Lang and Pryor, 1966) matches the speed exhibited by dolphins during their fastest breaches calculated in the present study. (Fish, 1998) recorded captive orca swimming up to 7.9 m/s, a speed that does not match the fastest breaching speed we calculated of 9 m/s. Extensive tabulations of cetacean swimming speeds are provided in Fish and Rohr (1999).

Maximum speed capabilities of larger fishes can be potentially recorded in the field, although sometimes tagged individuals do not exhibit such behaviour. For example, tagged blue marlin *Makaira nigricans*, at least 1 m long, were recorded swimming no faster than 2.25 m/s during 165 h of continuous tracking (Block et al., 1992). This may indicate that they did not hunt while tagged. In contrast, however, 1.5-m-long sailfish *Istiophorus platypterus* hunting sardines exhibited maximum speeds of 8.8 m/s (mean of top 3 fastest bursts; Marras et al., 2015; P. Domenici, pers. comm.). This speed is very close to the maximum breach speed observed for animals of a similar length in our dataset, and might suggest that during such hunts the sailfish are swimming close to their maximum speed. Devil rays *Mobula tarapacana*, about 3-m long (Thorrold, pers. comm.), reach speeds of up to 6 m/s during descents into the water column (Thorrold et al., 2014), while short-finned pilot whales *Globicephala melas*, 4 m in length, were recorded at mean maximum sprint speeds of 6 m/s (Aguilar Soto et al., 2008). These swimming speeds are commensurate with breaching speeds of similarly sized animals (Figure 1a). During burst swimming, tagged sperm whales *Physeter microcephalus*, between 6 and 10 m in length, were never observed swimming faster than 8 m/s (Aoki et al., 2012); this top speed is similar to that exhibited during breaches by the similarly sized orca and humpback

whale (Figure 1a). Spinner dolphins responding to an approaching ship reached swimming speeds up to 4.8 m/s (Au and Perryman, 1982) – considerably slower than the single fastest breach we recorded. Humpback whales have not been recorded in the wild swimming as fast as their most powerful breaches (e.g. 4.1 m/s; Williamson 1972).

Given that breaching speeds represented in our data set match the speeds of animals swimming in flumes designed to elicit maximum effort, and also match if not surpass the maximum swimming speeds of animals observed in the wild, the locomotion athleticism of fish and cetaceans during their fastest breaches may represent maximum capability. We conservatively estimate that the maximum mass-specific mechanical power exhibited by breaching species is about 35 to 50 W/kg of body mass (Figure 1b), though our calculations have assumed fin retraction, neutral buoyancy and that the animal is no longer accelerating just prior to breaching. Interestingly, this power production was attained by species across an order of magnitude in size from 20 cm to 2 m body length (very approximately 100 g to 100 kg) and as such may represent a power ceiling in general, based on an isometric relationship between maximum power and body mass within this range.

While we cannot fully validate our model estimating power, we can compare the resultant values to those in the literature obtained by alternate means. The fastest breaching species in our dataset were dolphins; our maximum power estimates for breaching dolphins are similar to the maximum fluke-beat-averaged value of 48 W/kg for the Pacific white-sided dolphin *Lagenorhynchus obliquidens* swimming at 7.4 m/s calculated by (Tanaka et al., 2019), the common bottlenose dolphin while tail standing (62.2 W/kg; Isogai, 2014) and porpoises *Stenella attenuata* encouraged to swim maximally fast along a 25-m course (50 W/kg; Lang and Pryor, 1966). Because the mass of the locomotor muscles is approximately half of the body mass (fao.org/3/T0219E/T0219E01.htm), and, at a given instant, only half of them are propelling the animal during the tail beat cycle, muscle power output at our estimated maximum is 140 to 200 W per kg. We therefore propose that these values represent an approximate maximum attainable power output by fish and cetaceans. And this is supported by the observation that 200W/kg muscle during fast flights in Phyllostomus bats (Thomas, 1975; Weis-Fogh and Alexander, 1977) and 214 W/kg of muscle exhibited by small lizards during vigorous movement Curtin et al. (2005) are the highest reported power output values we have found in the literature for any species within the size range of the breaching species represented in the current study (some higher values have been recorded for individual muscles; Table 1 in Josephson, 1993). Moreover, power output measurements for human participants requested to apply maximum effort at best match these values. For example, high-level rugby players

produced a mean peak power of 66.6 W/kg body mass during standing jumps (Tillin et al., 2013) - assuming 25 to 30 kg of leg muscle mass (Tillin, pers. comm.), their leg muscles were providing around 200 W/kg of power.

Valid estimates of maximum power are not only insightful physiologically, but in turn they elucidate an animal's behavioural limitations. In the case of breaching, for example, calculations of the necessary dimensions of dam spillways to enable fish to pass up them (Baigún et al., 2012; Beach, 1984) will greatly benefit from an understanding of breach velocity.

Author contributions

LGH and GI developed the ideas. LGH collected data; GI derived the equations and undertook the analyses. Both authors interpreted the results. LGH led on writing with input from GI.

Data availability

All data are included in the manuscript or the supplementary material.

Competing interests

We have no competing interests.

Ethical statement

Consent was not required.

Appendix A: A breaching event

Preliminaries

The information in this appendix details how to estimate the swimming speed of a breaching fish immediately before it has pierced the water surface, v_0. This problem, however, is not as trivial as it may appear. If the fish could have been approximated by a point mass, its air time τ' could have been correlated with the vertical speed on leaving the water, w_0', by

$$w_0' = g\tau'/2, \tag{A1}$$

where g is the acceleration of gravity. In turn, given the trajectory angle (relative to horizon) γ_0' at which the fish leaves the water, w_0' could have been correlated with take-off speed, v_0', by

$$v_0' = w_0'/\sin\gamma_0'. \tag{A2}$$

The fish, however, is not a point mass, and it likely gains energy (on the account of reduced wet area) between the moment when its nose (snout) pierces the water surface and the moment when its tail leaves the water. Consequently, the speed that the fish reaches immediately before piercing the water surface, v_0, is probably smaller than v_0'. Moreover, between the time the centre-of-mass leaves the water and the time the tail leaves the water, the motion of the fish is still assisted by buoyancy, and during that time, the fish decelerates at less than the acceleration of gravity. It increases the actual air time τ as compared with the air time τ' it would have had if it were a point mass leaving the water at v_0'. The aim of this appendix is to estimate the relations between τ and τ', and between v_0 and v_0'. To remain concise, the analysis will be based on the following seven assumptions:

1. The fish is neutrally buoyant;

2. It has reached a constant speed before piercing the water surface;

3. Its thrust (T) remains constant until the tail clears the water;

4. Its drag (*D*) is proportional to the wetted area and to the swimming speed squared;

5. Its body is symmetrical nose to tail;

6. Its fins (other than caudal) are contracted.

This list pertains to appendix B (the next one) as well.

Energy balance

Ignoring the resistance of air, the total mechanical energy of the fish E is preserved once its tail clears the water. During breaching, however, E is governed by

$$\frac{dE(x)}{dx} = T(x) - D\left(v^2(x), x\right),\tag{A3}$$

where $x \in (0, l)$ is the length of the fish above the water surface (l is the fork length), whereas $T(x)$ and $D(v^2, x)$ are thrust and drag of the (partially submerged) fish. Under assumptions 2 and 3,

$$T(x) = D\left(v^2(0), 0\right)\tag{A4}$$

for each $x \in (0, l)$. Under assumptions 4 and 6,

$$D\left(v^2(x), x\right) = v^2(x) D(1, x) = v^2(x) D(1, 0) \frac{S_w(x)}{S_w(0)},\tag{A5}$$

where, with $p(x)$ being the local girth,

$$S_w(x) = \int_x^l p(x') dx'\tag{A6}$$

is the respective wetted area. It is acknowledged that, in general, the drag comprises both form (pressure) and friction constituents (see appendix B), and therefore equation (A5) is coherent only if the form drag is small as compared with the friction drag.

Total mechanical energy of the fish is the sum

$$E(x) = E_p(x) + E_k(x)\tag{A7}$$

of the respective kinetic energy,

$$E_k(x) = mv^2(x)/2, \tag{A8}$$

and potential energy,

$$E_p(x) = \int_0^x \left(mg - B(x') \right) \sin \gamma(x') \, dx' \; ; \tag{A9}$$

it is tacitly assumed that kinetic energy associated with rotational motion is negligibly small as compared with the energy associated with translational motion.[1] In (A8) and (A9), m is the mass of the fish, g is the acceleration of gravity, γ is the breaching angle,

$$B(x) = \rho g \int_x^l s(x') \, dx' \tag{A10}$$

is the buoyancy of the submerged portion of the fish, $s(x)$ is the local cross section area of the fish, and, consistent with the assumption 1, ρ is the density of water;

$$B(0) = mg \tag{A11}$$

by assumption 1. We have tacitly assumed that the added mass (in the swimming direction) of a fusiform animal is negligibly small as compared with its 'real' mass (Iosilevskii et al, 2012).

Exploiting (A8), (A7), (A5) and (A4), equation (A3) can be recast as

$$\frac{dE(x)}{dx} + \frac{2}{m} E(x) D(1,x) = \frac{2}{m} E_k(0) D(1,0) + \frac{2}{m} E_p(x) D(1,x). \tag{A12}$$

Subject to the initial condition,

$$E(0) = E_k(0) = mv^2(0)/2 = mv_0^2/2 \tag{A13}$$

($E_p(0) = 0$ by (A9)), equation (A12) lends itself to a closed-form solution

---

[1] Kinetic energy associated with rotational motion is $k_a m r_y^2 \omega^2 / 2$ where r_y is the respective radius of gyration, ω is the angular velocity, and $k_a \in (1,2)$ is a certain parameter correcting for the added inertia effects. Typically, a jumping fish makes less than half a revolution per air time, but in this last case ω can be as high as π radians per second. For a double-ogive body, as the one described by (A43), $r_y = (2/7)l$, l being the length of the fish. Consequently, kinetic energy of the rotational motion can exceed the kinetic energy of translational motion when moving slower than approximately one body length per second. It can be ignored for a 1-m fish breaching at 6 m/s, but it cannot be ignored for a summersaulting 4-m great white breaching at the same speed.

$$E(x) = \frac{1}{F(x)} \left(E(0) + \frac{2}{m} \int_0^x \left(E(0) D(1,0) + E_{\mathrm{p}}(x') D(1,x') \right) F(x') dx' \right), \tag{A14}$$

in which

$$F(x) = \exp\left(\frac{2}{m} \int_0^x D(1,x') dx' \right). \tag{A15}$$

Velocity follows the energy by (A7)-(A8):

$$v^2(x) = \frac{2}{m} E_{\mathrm{k}}(x) = \frac{2}{m} \left(E(x) - E_{\mathrm{p}}(x) \right); \tag{A16}$$

the time to cross the water surface, nose-to-tail, $t(l)$, follows the velocity by quadrature,

$$t(x) = \int_0^x \frac{dx'}{v(x')}. \tag{A17}$$

Once the fish clears the water, it will return to the same height above water surface after

$$t_{\mathrm{free}} = \frac{2}{g} v(l) \sin \gamma(l) \tag{A18}$$

(compare with (A1)-(A2)). Whether or not the fish will touch the water at that point depends on the orientation of the body relative to horizon. To make the analysis simple, we will assume that it does touches the water at that point and therefore the time from piercing the surface on the way up to touching it on the way down is estimated at

$$\tau = t_{\mathrm{free}} + t(l) = \frac{2}{g} v(l) \sin \gamma(l) + \int_0^l \frac{dx'}{v(x')}. \tag{A19}$$

Possible error in (A19) stems from the assumption that the fish touches the water on the way back at the same height as it cleared the water on the way up. This height is $l \sin \gamma(l)$. If the fish has rotated in the air, it can land either vertically, in which case it will touch the water earlier, at height l, or it can land flat, in which case it will touch the water at height $d_{\mathrm{max}}/2$, where d_{max} is the maximal diameter of the body. Consequently, there can be an error $\Delta\tau$ in the flight time

$$\frac{l}{2v(l)}\big(\sin\gamma(l)-1\big) < \Delta\tau < \frac{l}{2v(l)}\bigg(\sin\gamma(l)-\frac{d_{\max}}{l}\bigg). \tag{A20}$$

Because τ is estimated from video footage of a breach by counting frames, the error can be reduced by extrapolating the fish trajectory and ending the frame count when the fish is approximately at the same height as when it has cleared the water; the frame count invariably starts when the fish pierces the water (Fig. A1).

Fish as a point mass

By definition, $E(l)$ is the mechanical energy of the fish when it clears the water. It is preserved afterwards, until the fish touches the water again on its way back – in fact, it is the basis underlying (A18). By extension, it is also the mechanical energy of the fish, if it were a point mass, on crossing the water surface on the way up. Because the potential energy of a point-mass-fish is zero at the surface, its effective take-off speed and angle are

$$v_0'^2 = v^2(0)\frac{E(l)}{E(0)}, \tag{A21}$$

$$\gamma_0' = \cos^{-1}\frac{v(l)\cos\gamma(l)}{v_0'}; \tag{A22}$$

the last equation is based on the notion that horizontal velocity component, $v\cos\gamma$, remains constant during a free flight. Both parameters are different from the respective speed $v(l/2)$ and angle $\gamma(l/2)$ at the time the centre-of-mass of the 'real' fish crosses the surface – recall that during a breach, motion of the 'real' fish is assisted by thrust and buoyancy. Likewise, the flight time of the point mass fish,

$$\tau' = \frac{2}{g}v_0'\sin\gamma_0' = \frac{2}{g}\sqrt{v_0'^2 - v^2(l)\cos^2\gamma(l)}, \tag{A23}$$

differs, at least in principle, from the flight time τ of the 'real' fish.

Dimensionless form

The above formulae are hardly simple, and have to be simplified to become practical. To this end, it will prove convenient to introduce dimensionless quantities. Represented by overbars, we set

$$\bar{x} = \frac{x}{l}, \qquad \bar{t} = \frac{t v_0}{l}, \qquad \bar{p}(\bar{x}) = \frac{p(\bar{x}l)}{l}, \qquad \bar{s}(\bar{x}) = \frac{s(\bar{x}l)}{l^2}, \qquad \text{(A24)}$$

$$\bar{v}(\bar{x}) = \frac{v(\bar{x}l)}{v(0)}, \qquad \bar{B}(\bar{x}) = \frac{B(\bar{x}l)}{B(0)}, \qquad \bar{D}(\bar{x}) = \frac{D(1,\bar{x}l)}{D(1,0)}, \qquad \text{(A25)}$$

$$\bar{E}(\bar{x}) = \frac{E(\bar{x}l)}{E(0)}, \qquad \bar{E}_k(\bar{x}) = \frac{E_k(\bar{x}l)}{E(0)}, \qquad \bar{E}_p(\bar{x}) = \frac{E_p(\bar{x}l)}{E(0)}. \qquad \text{(A26)}$$

Thus, with

$$\bar{A} = \frac{2}{m} D(1,0) l, \qquad \text{(A27)}$$

$$\mathrm{Fr}_0 = v_0 \Big/ \sqrt{gl}, \qquad \text{(A28)}$$

equations (A5), (A6), (A10), (A14), (A15), (A9), (A16), (A17) and (A18) take on the respective forms

$$\bar{D}(\bar{x}) = \left(\int_{\bar{x}}^{1} \bar{p}(\bar{x}') d\bar{x}' \right) \left(\int_{0}^{1} \bar{p}(\bar{x}') d\bar{x}' \right)^{-1} \qquad \text{(A29)}$$

$$\bar{B}(\bar{x}) = \left(\int_{\bar{x}}^{1} \bar{s}(\bar{x}') d\bar{x}' \right) \left(\int_{0}^{1} \bar{s}(\bar{x}') d\bar{x}' \right)^{-1} \qquad \text{(A30)}$$

$$\bar{E}(\bar{x}) = \frac{1}{\bar{F}(\bar{x})} \left(1 + \bar{A} \int_{0}^{\bar{x}} \left(1 + \bar{E}_p(\bar{x}') \bar{D}(\bar{x}') \right) \bar{F}(\bar{x}') d\bar{x}' \right), \qquad \text{(A31)}$$

$$\bar{F}(\bar{x}) = \exp\left(\bar{A} \int_{0}^{\bar{x}} \bar{D}(\bar{x}') d\bar{x}' \right), \qquad \text{(A32)}$$

$$\bar{E}_p(\bar{x}) = \frac{2}{\mathrm{Fr}_0^2} \int_{0}^{\bar{x}} \left(1 - \bar{B}(\bar{x}') \right) \sin \gamma(\bar{x}') d\bar{x}', \qquad \text{(A33)}$$

$$\bar{v}^2(\bar{x}) = \bar{E}_k(\bar{x}) = \bar{E}(\bar{x}) - \bar{E}_p(\bar{x}), \qquad \text{(A34)}$$

$$\bar{t}(\bar{x}) = \int_0^{\bar{x}} \frac{d\bar{x}'}{\bar{v}(\bar{x}')} = \int_0^{\bar{x}} \frac{d\bar{x}'}{\sqrt{\bar{E}_k(\bar{x}')}} , \tag{A35}$$

$$\bar{t}_{free} = 2Fr_0^2 \bar{v}(1)\sin\bar{\gamma}(1) = 2Fr_0^2 \sin\bar{\gamma}(1)\sqrt{\bar{E}_k(1)} . \tag{A36}$$

Likewise,

$$\bar{v}_0'^2 = \bar{E}(1) , \tag{A37}$$

$$\bar{\tau}' = 2Fr_0^2 \sqrt{\bar{E}(1) - \bar{E}_k(1)\cos^2\bar{\gamma}(1)} \tag{A38}$$

by (A21) and (A23).

Approximate solution

Recalling that the accuracy of capturing the flight time is a few percent at best (one frame count

at 30 frames/s for flight time of the order of 1 s), we seek a simplified (approximate) variant of

the above formulae.

Drag of the fish can always be expressed in terms of its drag coefficient C_D as

$$D(1,0) = \frac{1}{2}\rho S_{max} C_D , \tag{A39}$$

where $S_{max} = \max_{x \in (0,l)} s(x)$ is the maximal cross section area of the fish. Consequently,

$$\bar{A} = C_D / k_{pc} \tag{A40}$$

by (A27), where

$$k_{pc} = \frac{m}{\rho S_{max} l} \tag{A41}$$

is equivalent to the prismatic coefficient – the ratio between the volume of fish and the volume

of the minimal cylinder enclosing it. Typically, C_D is a small number of the order of 0.1

(appendix B), whereas k_{pc} is invariably bounded between 0.5 and 0.6 (it is $8/15$ for a double-

ogive body, as the one described by (A43) below). Consequently, $\bar{A}$ can be considered a small

parameter, furnishing (A31) in asymptotic form,

$$\bar{E}(\bar{x}) = 1 + \bar{A}\int_0^{\bar{x}}(1-\bar{D}(\bar{x}'))d\bar{x}' + \bar{A}\int_0^{\bar{x}}\bar{E}_{\mathrm{p}}(\bar{x}')\bar{D}(\bar{x}')d\bar{x}' + O(\bar{A}^2). \tag{A42}$$

Next, we assume that the body of a fish is, indeed, a double-ogive, whereby its effective diameter d changes along the fish as

$$\bar{d}(\bar{x}) = 4\bar{d}_{\max}\bar{x}(1-\bar{x}), \tag{A43}$$

where $\bar{d}_{\max} = \sqrt{4S_{\max}/\pi l^2}$. In this case, one will readily find

$$\bar{D}(\bar{x}) = \left(\int_{\bar{x}}^1 \bar{d}(\bar{x})dx'\right)\left(\int_0^1 \bar{d}(\bar{x})dx'\right)^{-1} = 1 - 3\bar{x}^2 + 2\bar{x}^3, \tag{A44}$$

$$\bar{B}(\bar{x}) = \left(\int_{\bar{x}}^1 \bar{d}^2(\bar{x})dx'\right)\left(\int_0^1 \bar{d}^2(\bar{x})dx'\right)^{-1} = 1 - 10\bar{x}^3 + 15\bar{x}^4 - 6\bar{x}^5, \tag{A45}$$

$$\int_0^{\bar{x}}(1-\bar{D}(1,\bar{x}'))d\bar{x}' = \bar{x}^3 - \frac{1}{2}\bar{x}^4. \tag{A46}$$

Noting the positive-definiteness of the respective integrands, we can pull $\sin\gamma$ out of the integral sign in (A33) and (A42) to obtain

$$\bar{E}_{\mathrm{p}}(\bar{x}) = \frac{\sin\bar{\gamma}(\bar{x}_*)}{\mathrm{Fr}_0^2}\bar{x}^4(5 - 6\bar{x} + 2\bar{x}^2), \tag{A47}$$

$$\int_0^{\bar{x}}\bar{E}_{\mathrm{p}}(\bar{x}')\bar{D}(\bar{x}')d\bar{x}' = \frac{\sin\bar{\gamma}(\bar{x}_+)}{\mathrm{Fr}_0^2}\bar{I}_{\mathrm{p}}(\bar{x}), \tag{A48}$$

where

$$\bar{I}_{\mathrm{p}}(\bar{x}) = \bar{x}^5\left(1 - \bar{x} - \frac{13}{7}\bar{x}^2 + \frac{7}{2}\bar{x}^3 - 2\bar{x}^4 + \frac{2}{5}\bar{x}^5\right) \tag{A49}$$

and in which $\bar{x}_*$ and $\bar{x}_+$ are certain points in the interval $(0,\bar{x})$. Consequently,

$$\bar{E}(\bar{x}) = 1 + \bar{A}\left(\left(\bar{x}^3 - \frac{1}{2}\bar{x}^4\right) + \frac{\sin\bar{\gamma}(\bar{x}_+)}{\mathrm{Fr}_0^2}\bar{I}_{\mathrm{p}}(\bar{x})\right) + O(\bar{A}^2). \tag{A50}$$

Fortuitously, the ratio of the second term in the parentheses to the first does not exceed

$0.135/\mathrm{Fr}_0^2$ for any $\bar{x} \in (0,1)$. Consequently, it can be conveniently neglected as compared with the first, leaving

$$\bar{E}(\bar{x}) \approx 1 + \bar{A}\bar{x}^3 \frac{2-\bar{x}}{2} \tag{A51}$$

independent of the pre-breaching Froude number Fr_0 (it is tacitly assumed that as the Froude number is of the order of unity – otherwise the shark would not have been able to clear the tail out of the water).

The instantaneous (reduced) velocity, $\bar{v}(\bar{x}) = \sqrt{\bar{E}_k(\bar{x})}$, is given by (A34), but even with (A51), $\bar{E}_k(\bar{x})$ is still a sixth-order polynomial, and hence cannot be easily integrated in (A35) to obtain the crossing time, $\bar{t}(1)$. To this end, we suggest approximating $\bar{E}_k$ and $\bar{E}$ by

$$\bar{E}_k(\bar{x}) \approx 1 + 2\left(\frac{\bar{A}}{2} - \frac{\sin \bar{\gamma}(1)}{\mathrm{Fr}^2}\right)\left(\bar{x} - \frac{1}{2}\right)\mathrm{H}\left(\bar{x} - \frac{1}{2}\right), \tag{A52}$$

$$\bar{E}(\bar{x}) \approx 1 + \bar{A}\left(\bar{x} - \frac{1}{2}\right)\mathrm{H}\left(\bar{x} - \frac{1}{2}\right), \tag{A53}$$

which fit both the values and the derivatives of $\bar{E}_k$ and $\bar{E}$ at 0 and 1 (replacing $\bar{\gamma}(\bar{x}_*)$ by $\bar{\gamma}(1)$ is consistent with the order of the approximation). Here, H stands for the Heaviside step function. They manifest the notion that the energy is gained only after the centre of mass has raised above the water, and up to that point the velocity remains practically constant (in fact, $\bar{E}_p(1/2) = (5/32)\bar{E}_p(1)$ and $\left(\bar{E}(1/2) - \bar{E}(0)\right) \approx (3/16)\left(\bar{E}(1) - \bar{E}(0)\right)$ by (A47) and (A51)). They yield

$$\bar{t}(1) \approx \frac{1}{2} + \frac{1 - \sqrt{\bar{E}_k(1)}}{1 - \bar{E}_k(1)} = \frac{1}{2} + \frac{1}{1 + \sqrt{\bar{E}_k(1)}} \tag{A54}$$

for the crossing time. The accuracy of (A52)-(A54) can be assessed from Figs. A2a-c.

The flight time, measured between the time that the nose pierces the water on the way up and the time when some part of the fish touches the water on the way back, is

$$\overline{\tau} = \overline{t}(1) + 2\mathrm{Fr}_0^2 \overline{v}(1) \sin \overline{\gamma}(1) = \frac{1}{2} + \frac{1}{1 + \sqrt{\overline{E}_k(1)}} + 2\mathrm{Fr}_0^2 \sqrt{\overline{E}_k(1)} \sin \overline{\gamma}(1) \qquad (A55)$$

by (A54) and (A36). Its asymptotic series with respect to $\left(\mathrm{Fr}^2 \sin \overline{\gamma}(1)\right)^{-1}$ and $\overline{A}$ is

$$\overline{\tau} = 2\mathrm{Fr}_0^2 \sin \overline{\gamma}(1) \left(1 + \frac{1}{4} \overline{A} \right) + \cos^2 \overline{\gamma}(1) + \ldots, \qquad (A56)$$

where the ellipsis stands for terms of the order $\left(\mathrm{Fr}^2 \sin \overline{\gamma}(1)\right)^{-1}$ and $\overline{A}$. The accuracy of this approximation can be assessed from Fig. A2d.

By comparison, the air time of a point-mass fish (from the point it leaves the water until the points it enters it again) is

$$\overline{\tau}' = 2\mathrm{Fr}_0^2 \sqrt{\overline{E}(1) - \overline{E}_k(1) \cos^2 \overline{\gamma}(1)} \qquad (A57)$$

Its asymptotic series with respect to $\left(\mathrm{Fr}^2 \sin \overline{\gamma}(1)\right)^{-1}$ and $\overline{A}$ is remarkably the same as (A56)

$$\overline{\tau}' = 2\mathrm{Fr}_0^2 \sin \overline{\gamma}(1) \left(1 + \frac{\overline{A}}{4} \right) + \cos^2 \overline{\gamma}(1) + \ldots. \qquad (A58)$$

Recalling that

$$\overline{\tau} = \tau v_0 / l = \tau \mathrm{Fr} \sqrt{g/l} \qquad (A59)$$

by definition (A24), equation (A56) actually furnishes a quadratic equation for Fr, which has an obvious solution,

$$\mathrm{Fr} = \frac{1}{4 \sin \overline{\gamma}(1) \left(1 + \frac{1}{4} \overline{A} \right)} \sqrt{\frac{g\tau^2}{l}} \left(1 + \sqrt{1 - \frac{8l}{g\tau^2} \sin \overline{\gamma}(1) \cos^2 \overline{\gamma}(1) \left(1 + \frac{1}{4} \overline{A} \right)} \right). \qquad (A60)$$

Its asymptotic form is

$$\mathrm{Fr} = \frac{1}{2 \sin \overline{\gamma}(1)} \sqrt{\frac{g\tau^2}{l}} \left(1 - \frac{1}{4} \overline{A} - \frac{2l}{g\tau^2} \sin \overline{\gamma}(1) \cos^2 \overline{\gamma}(1) + \ldots \right), \qquad (A61)$$

where the ellipsis stands for terms of the order $\left(g\tau^2 / l\right)^{-2}$, $\overline{A}^2$ and $\left(g\tau^2 / l\right)^{-1} \overline{A}$ (Fig. A3). The

formula that relates v_0 and τ,

$$v_0 = \frac{g\tau}{2\sin\bar{\gamma}(1)}\left(1 - \frac{1}{4}\bar{A}\right) - \frac{l}{\tau}\cos^2\bar{\gamma}(1) + \ldots, \tag{A62}$$

follows (A61) by (A28). The two correcting factors are the energy added due to reduced drag – this is the coefficient $\left(1 - \bar{A}/4\right)$ in the first term – and trajectory angle correction, manifested in the last term.

Appendix B: Swimming power

Drag coefficient

Estimation of the drag coefficient will be based on aircraft preliminary design tools compiled in Raymer (1992). They have already been used to the same end in Iosilevskii and Papastamatiou (2016), and they are briefly recapitulated here. Having assumed that the fish has no retracted fins (this ensures that the drag estimate furnishes the lower bound of possible drag) and having assumed that the fish is neutrally buoyant, its drag coefficient based on the maximal cross section area,

$$S_{\max} = (\pi/4)d_{\max}^2, \tag{B1}$$

is

$$C_D = \frac{S_{\mathrm{w}}}{S_{\max}} f\left(d_{\max}/l\right) C_f\left(\mathrm{Re}\right), \tag{B2}$$

where S_{w} is the wet surface area of the body, $d_{\max}$ is the maximal effective diameter,

$$f\left(\bar{d}\right) \approx 1 + 60\bar{d}^3 + \frac{1}{400\bar{d}} \tag{B3}$$

if the form factor manifesting the effect of the pressure drag,

$$\mathrm{Re} = \rho v_0 l/\mu \tag{B4}$$

is the respective Reynolds number based on the body length (μ stands for the viscosity of water), and C_f is the respective friction coefficient, which can be approximated by

$$C_f\left(\mathrm{Re}\right) \approx \frac{0.454}{\left(\log_{10}\mathrm{Re}\right)^{2.58}}, \tag{B5}$$

if the boundary layer on the body is mostly turbulent, and by

$$C_f(\text{Re}) \approx \frac{1.33}{\sqrt{\text{Re}}}, \tag{B6}$$

if the boundary layer is mostly laminar (Raymer, 1992). At Reynolds numbers in excess of, say, 10^5, we render the boundary layer over scaled surface turbulent.

For a double ogive body, as the one described by (A43),

$$S_w = (2\pi/3) d_{max} l ; \tag{B7}$$

and, consequently,

$$C_D = \frac{8}{3} \frac{f(d_{max}/l)}{d_{max}/l} C_f(\text{Re}), \tag{B8}$$

The coefficient with C_f is shown on figure B1. Because most fish have d_{max}/l in the range $(0.15, 0.25)$, it can be closely approximated by 20. In other words, the drag coefficient of a finless fish approximates by

$$C_D \approx 20 C_f(\text{Re}), \tag{B9}$$

irrespective of its body proportions. With $k_{pc} = 8/15$, the ratio, $\bar{A} = C_D/k_{pc}$, introduced in (A40), approximates by

$$\bar{A} \approx (75/2) C_f(\text{Re}). \tag{B10}$$

Having multitude of non-retractable fins, sharks probably represent the most hydrodynamically 'dirty' of the fusiform fish. At zero lift, their drag coefficient exceeds the estimate of (B9) by about 30% (Iosilevskii and Papastamatiou, 2016).

Swimming power
Mechanical power needed to overcome hydrodynamic resistance is given by

$$P = \frac{1}{\eta_h} D(v_0^2, 0) v_0 = \frac{1}{\eta_h} D(1, 0) v_0^3 \tag{B11}$$

where η_h is the effective propulsion efficiency (Iosilevskii and Papastanatiou, 2016). The

expression on the right was obtained with the help of (A5). The value of η_h is controversial, probably because of the inherent difficulty in separating the drag and thrust of a self-propelling body. Theoretical predictions put it between 0.8 and 0.9 (Chopra and Kambe, 1977); more accurate analysis put it between 0.8 and 0.85 (Liu and Bose, 1997) The effective mass-specific power

$$\frac{P}{m} = \frac{1}{\eta_h} \frac{D(1,0)}{m} v_0^3 = \frac{\overline{A}}{2\eta_h} \frac{v_0^3}{l} \tag{B12}$$

follows (B11) by (A27).

Appendix C: Estimation errors

The set of logarithmic derivatives,

$$\frac{\partial \ln v_0}{\partial \ln \overline{A}} = -\frac{\overline{A}}{v_0} \frac{g\tau}{8\sin\overline{\gamma}(1)} = -\frac{\overline{A}}{4}\left(1 + \frac{l}{\tau v_0}\cos^2\overline{\gamma}(1) + \ldots\right), \tag{C1}$$

$$\frac{\partial \ln v_0}{\partial \ln l} = -\frac{l}{\tau v_0}\cos^2\overline{\gamma}(1) + \ldots, \tag{C2}$$

$$\frac{\partial \ln v_0}{\partial \ln \tau} = 1 + \frac{2l}{\tau v_0}\cos^2\overline{\gamma}(1) + \ldots, \tag{C3}$$

$$\frac{\partial \ln v_0}{\partial \overline{\gamma}(1)} = \cot\overline{\gamma}(1)\left(-1 + \frac{l}{\tau v_0}\left(2 - 3\cos^2\overline{\gamma}(1)\right) + \ldots\right), \tag{C4}$$

$$\frac{\partial \ln(P/m)}{d\ln\overline{A}} = 1 + 3\frac{\partial \ln v_0}{d\ln\overline{A}} \approx 1, \tag{C5}$$

$$\frac{\partial \ln(P/m)}{d\ln l} = -1 + 3\frac{\partial \ln v_0}{d\ln l}, \tag{C6}$$

$$\frac{\partial \ln(P/m)}{d\ln\tau} = 3\frac{\partial \ln v_0}{\partial \ln\tau}, \tag{C7}$$

$$\frac{\partial \ln(P/m)}{d\overline{\gamma}(1)} = 3\frac{\partial \ln v_0}{\partial \overline{\gamma}(1)}, \tag{C8}$$

which immediately follow from (A62) and (B12), relate the uncertainties in v_0 and P/m with

uncertainties in $\overline{A}$, τ, $\overline{\gamma}(1)$ and l. They are shown in Fig. C1. Typical values of $\overline{A}$, τ, $\overline{\gamma}(1)$ and l were 0.1, 1 s, 1 rad and 1 m, respectively. They yield v_0 between 5 and 10 m/s, rendering the combination $l/\tau v_0$ to be bounded to the interval (0.1, 1). We estimate that uncertainties in $\overline{A}$, τ, $\overline{\gamma}(1)$ and l are 30%, 3%, 1/4 rad (15°), and 30%, respectively. The uncertainty in $\overline{A}$ is associated mainly with the uncertainty in the wetted area; the uncertainty in τ was taken to be one frame (at 30 frames/s); the uncertainty in $\overline{\gamma}(1)$ is guessed based on observations, and the uncertainty in l stems directly from our taking a typical length of a species instead of the particular one. Toward what follows (but not in the text), it will be tacitly assumed that the uncertainties in l and in $\overline{A}$ are independent.

Based on (C1), a 30% uncertainty in $\overline{A}$ has practically no effect on v_0 (less than 1%). Based on (C2), a 30% uncertainty in length has no effect on v_0 if the breach is near vertical (say, above 75°), but can lead to a large uncertainty if the animal is large (e.g. 5 m) and breaches at a shallow angle (Fig C1a). Based on (C3), a 3% uncertainty in the air time yields a 3% to 6% uncertainty in v_0 (see Fig. C1c). Based on (C4), a quarter-radian uncertainty in the breaching angle has no effect on v_0 when the animal breaches almost vertically, but can render the estimate of v_0 unreliable when the breaching angle becomes less than about 60° (see Fig. C1e).

Being dependent on v_0^3, the uncertainties in P/m are naturally larger than those in v_0. In particular, uncertainties of 30% in length and in $\overline{A}$ are reflected in comparable uncertainties in P/m – see (C5), (C6), (C1) and (C2). A 3% uncertainty in the air time yields 9% to 18% uncertainty in P/m – see (C7), (C3) and Fig. C1d. Perhaps the biggest uncertainty is associated

with the breaching angle – see (C8), (C4) and Fig. C1f; it can be reduced by considering only those cases where the breaching angle exceeds 70-75°.

Appendix D: Lesser devil ray

A mobulid ray do not fit the assumptions underlying the preceding Appendices. Because its propulsion does not come from the caudal end, it is plausible that it does not accelerate when crossing the water surface. It renders the correction factors in (A62) redundant, leaving

$$v_0 = \frac{g\tau}{2\sin\bar{\gamma}(1)} + \ldots \tag{D1}$$

as a simple leading order approximation for the breaching speed. Its drag coefficient is also different. With S being the planform area, it can be estimated with

$$C_D \approx f' \frac{S_w}{S_{max}} C_f(\mathrm{Re}), \tag{D2}$$

where S_w is the surface area and f' is an empirical correction accounting for drag due to separation of the boundary layer. In principle, f' depends on the thickness to chord ratio of the ray, but because it changes dramatically across the span (width) of the ray, it is difficult to assess. We will take it, cautiously, as 1.2 by equation (12.30) in Raymer (1992).

Mobulid rays are practically diamond shaped, and hence

$$S_w \approx wl, \tag{D3}$$

where w is the width. Assuming that the proportions of the animal's body do not change with length, we can set

$$w = \bar{w}l \text{ and } m = \rho\bar{m}l^3, \tag{D4}$$

which closely fit the available morphological data (provided courtesy of Chris Lawson) with $\bar{w} = 1.7$ and $\bar{m} = 0.06$ (see Fig. D1). Thus,

$$\frac{P}{m} = \frac{\bar{w}}{\bar{m}} f' C_f(\mathrm{Re}) \frac{1}{2\eta_h} \frac{\bar{v}_0^3}{l} \tag{D5}$$

by (B11), (D4), (D3) and (D2). Comparison between (D5) and (B12) yields

$$\bar{A} = \frac{\bar{w}}{\bar{m}} f' C_f(\mathrm{Re}) \approx 34 C_f(\mathrm{Re}), \tag{D6}$$

which is practically the same as in (B10). The analysis in the text was based on the latter.

References

Chopra, M.G. and Kambe, T., 1977, "Hydromechanics of lunate-tail swimming propulsion. Part 2," *Journal of Fluid Mechanics* **79**(1), pp. 49-69.

Iosilevskii G., Papastamatiou Y.P., Meyer C.G., and Holland K.N., 2012, "Energetics of the yo-yo dives of predatory sharks," *Journal of Theoretical Biology* **294**, pp. 172–181.

Iosilevskii G. and Papastamatiou Y.P., 2016, "Relations between morphology, buoyancy and energetics of requiem sharks," *Royal Society Open Science* **3**: 160408.

Liu P. and Bose N., 1997, "Propulsive performance from oscillating propulsors with spanwise flexibility," *Proceedings of the Royal Society of London* A **453**, pp. 1763-1770

Raymer D.P., 1992, *Aircraft design: a conceptual approach*, AIAA educational series, Washington DC, pp 279-281

References

Aguilar Soto, N., Johnson, M. P., Madsen, P. T., Díaz, F., Domínguez, I., Brito, A. and Tyack, P. (2008). Cheetahs of the deep sea: deep foraging sprints in short-finned pilot whales off Tenerife (Canary Islands). *Journal of Animal Ecology* **77**, 936-947.

Aoki, K., Amano, M., Mori, K., Kourogi, A., Kubodera, T. and Miyazaki, N. (2012). Active hunting by deep-diving sperm whales: 3D dive profiles and maneuvers during bursts of speed. *Marine Ecology Progress Series* **444**, 289-301.

Au, D. and Perryman, W. (1982). Movement and speed of dolphin schools responding to an approaching ship. *Fishery Bulletin* **80**, 371-379.

Baigún, C. R., Nestler, J. M., Minotti, P. and Oldani, N. (2012). Fish passage system in an irrigation dam (Pilcomayo River basin): When engineering designs do not match ecohydraulic criteria. *Neotropical Ichthyology* **10**, 741-750.

Beach, M. (1984). Fish pass design-criteria for the design and approval of fish passes and other structures to facilitate the passage of migratory fish in rivers. In *Fisheries Research Technial Report No. 78*. Lowestoft, UK: Ministry of Agriculture, Fisheries and Food.

Block, B. A., Booth, D. and Carey, F. G. (1992). Direct measurement of swimming speeds and depth of blue marlin. *Journal of Experimental Biology* **166**, 267-284.

Castro-Santos, T., Sanz-Ronda, F. J. and Ruiz-Legazpi, J. (2012). Breaking the speed limit — comparative sprinting performance of brook trout (*Salvelinus fontinalis*) and brown trout (*Salmo trutta*). *Canadian Journal of Fisheries and Aquatic Sciences* **70**, 280-293.

Chopra, M. and Kambe, T. (1977). Hydromechanics of lunate-tail swimming propulsion. Part 2. *Journal of Fluid Mechanics* **79**, 49-69.

Curtin, N. A., Woledge, R. C. and Aerts, P. (2005). Muscle directly meets the vast power demands in agile lizards. *Proceedings of the Royal Society B: Biological Sciences* **272**, 581-584.

Fish, F. (1998). Comparative kinematics and hydrodynamics of odontocete cetaceans: morphological and ecological correlates with swimming performance. *Journal of Experimental Biology* **201**, 2867-2877.

Fish, F. E. and Rohr, J. (1999). Review of dolphin hydrodynamics and swimming performance: Space and naval warfare systems command. San Diego CA.

Husak, J. F., Fox, S. F., Lovern, M. B. and Bussche, R. A. V. D. (2006). Faster lizards sire more offspring: sexual selection on whole-animal performance. *Evolution* **60**, 2122-2130.

Iosilevskii, G. and Papastamatiou, Y. P. (2016). Relations between morphology, buoyancy and energetics of requiem sharks. *Royal Society Open Science* **3**, 160406.

Isogai, K. (2014). Effect of flexibility of the caudal fin on the propulsive performance of dolphins. *Transactions of the Japan Society for Aeronautical and Space Sciences* **57**, 21-30.

Johnston, E. M., Halsey, L. G., Payne, N. L., Kock, A. A., Iosilevskii, G., Whelan, B. and Houghton, J. D. R. (2018). Latent power of basking sharks revealed by exceptional breaching events. *Biology Letters* **14**.

Josephson, R. (1993). Contraction dynamics and power output of skeletal muscle. *Annual Review of Physiology* **55**, 527-546.

Kyle, C. R. (1986). Experiments in human ergometry as applied to the design of human powered vehicles. *Journal of Applied Biomechanics* **2**, 6-19.

Lang, T. G. and Pryor, K. (1966). Hydrodynamic performance of porpoises (*Stenella attenuata*). *Science* **152**, 531-533.

Liu, P. and Bose, N. (1997). Propulsive performance from oscillating propulsors with spanwise flexibility. *Proceedings of the Royal Society of London. Series A: Mathematical, Physical and Engineering Sciences* **453**, 1763-1770.

Lutcavage, M., Brill, R., Skomal, G., Chase, B., Goldstein, J. and Tutein, J. (2000). Tracking adult North Atlantic bluefin tuna (*Thunnus thynnus*) in the northwestern Atlantic using ultrasonic telemetry. *Marine Biology* **137**, 347-358.

Marras, S., Noda, T., Steffensen, J. F., Svendsen, M. B., Krause, J., Wilson, A. D., Kurvers, R. H., Herbert-Read, J., Boswell, K. M. and Domenici, P. (2015). Not so fast: swimming behavior of sailfish during predator–prey interactions using high-speed video and accelerometry. *Integrative and Comparative Biology* **55**, 719-727.

Matthes, H. (1977). The problem of rice-eating fish in the central Niger Delta, Mali. In *Symposium on River and Floodplain Fisheries, Bujumbura (Burundi)*, pp. 225-252. Bujumbura: FAO/CIFA.

Parsons, G. R., Stell, E. and Hoover, J. J. (2016). Estimating burst swim speeds and jumping characteristics of silver carp (*Hypophthalmichthys molitrix*) using video analyses and principles of projectile physics: US Army Engineer Research and Development Center Vicksburg United States.

Perez-Gomez, J., Rodriguez, G. V., Ara, I., Olmedillas, H., Chavarren, J., González-Henriquez, J. J., Dorado, C. and Calbet, J. A. L. (2008). Role of muscle mass on sprint performance: gender differences? *European Journal of Applied Physiology* **102**, 685-694.

Rohr, J., Fish, F. and Gilpatrick Jr, J. (2002). Maximum swim speeds of captive and free-ranging delphinids: Critical analysis of extraordinary performance. *Marine Mammal Science* **18**, 1-19.

Sanz-Ronda, F. J., Ruiz-Legazpi, J., Bravo-Córdoba, F. J., Makrakis, S. and Castro-Santos, T. (2015). Sprinting performance of two Iberian fish: *Luciobarbus bocagei*

and *Pseudochondrostoma duriense* in an open channel flume. *Ecological Engineering* **83**, 61-70.

Semmens, J. M., Kock, A. A., Watanabe, Y. Y., Shepard, C. M., Berkenpas, E., Stehfest, K. M., Barnett, A. and Payne, N. L. (2019). Preparing to launch: biologging reveals the dynamics of white shark breaching behaviour. *Marine Biology* **166**, 95.

Sepulveda, C., Graham, J. and Bernal, D. (2007). Aerobic metabolic rates of swimming juvenile mako sharks, *Isurus oxyrinchus*. *Marine Biology* **152**, 1087-1094.

Tanaka, H., Li, G., Uchida, Y., Nakamura, M., Ikeda, T. and Liu, H. (2019). Measurement of time-varying kinematics of a dolphin in burst accelerating swimming. *PLoS ONE* **14**, e0210860.

Thomas, S. (1975). Metabolism during flight in two species of bats, *Phyllostomus hastatus* and *Pteropus gouldii*. *Journal of Experimental Biology* **63**, 273-293.

Thorrold, S. R., Afonso, P., Fontes, J., Braun, C. D., Santos, R. S., Skomal, G. B. and Berumen, M. L. (2014). Extreme diving behaviour in devil rays links surface waters and the deep ocean. *Nature Communications* **5**.

Tillin, N. A., Pain, M. T. G. and Folland, J. (2013). Explosive force production during isometric squats correlates with athletic performance in rugby union players. *Journal of Sports Sciences* **31**, 66-76.

Videler, J. and Wardle, C. (1991). Fish swimming stride by stride: speed limits and endurance. *Reviews in Fish Biology and Fisheries* **1**, 23-40.

Watanabe, Y. Y., Wei, Q., Du, H., Li, L. and Miyazaki, N. (2013). Swimming behavior of Chinese sturgeon in natural habitat as compared to that in a deep reservoir: preliminary evidence for anthropogenic impacts. *Environmental Biology of Fishes* **96**, 123-130.

Weis-Fogh, T. and Alexander, R. M. (1977). The sustained power output from striated muscle. In *Scale Effects in Animal Locomotion*, (ed. J. Pedley), pp. 511-525. London: Academic Press.

Wilson, R. S., Husak, J. F., Halsey, L. G. and Clemente, C. J. (2015). Predicting the movement speeds of animals in natural environments. *Integrative and Comparative Biology* **55**, 1125-1141.

Table 1. The fastest three breaches of the species included in the analyses, from the data compiled from the listed data sources. Approximate timings of those fastest breaches in the data sources are provided where appropriate.

Species	N	l (m)	τ (s)	γ (°)	A	v_0 (m/s)	P/m (W/kg)	Video	length (l)
								Data sources	
African tetra[1] Genus: *Alestes*	-	0.2	0.90	90	0.17	4.4	36.2	(Matthes, 1977)	FishBase
Basking shark† *Cetorhinus maximus*	13	6.4	1.2 1.1 1.0	80 80 80	0.09 0.09 0.09	6.0 5.5 5.2	1.5 1.1 0.9	The dataset published in (Johnston et al., 2018)	FishBase
Common bottlenose dolphin[2] Genus: *Tursiops*	9	2.2	2.24 2.20 2.08	90 80 90	0.10 0.10 0.10	10.7 10.7 10.0	30.4 29.9 24.6	Youtube https://www.youtube.com/watch?v=swsfdv2jhbc https://www.youtube.com/watch?v=m3tZxo8ljL4 07:18, 09:38, 10.25 https://www.youtube.com/watch?v=Sfb8wtAdy1o	Wikipedia
Gulf sturgeon *Acipenser oxyrinchus desotoi*	5	1.5	1.28 1.12 1.12	90 90 90	0.11 0.12 0.12	6.3 5.5 5.8	9.5 6.5 6.5	Youtube https://www.youtube.com/watch?v=oSC0AZ5_0F8 00:16, 00:29, 00:48 https://www.youtube.com/watch?v=e1a_mBGLucQ	Visual assessment of videos
Harbour porpoise *Phocoena phocoena*	9	1.65	1.44 1.44	70 80	0.11 0.11	7.5 7.2	13.5 12.3	Youtube Video ('*Wild Dolphins Jumping* New Zealand,	Wikipedia

			1.40	75	0.11	7.1	11.8	Kaikoura') currently unavailable online. 00:03, 01:15, 02:23	
Humpback whale† *Megaptera novaeangliae*	20	13.0	1.83 1.76 1.70	80 90 90	0.08 0.08 0.08	9.1 8.6 8.3	2.2 2.0 1.8	Youtube https://www.youtube.com/watch?v=ZLkWGNs2Yc0&t=39s https://www.youtube.com/watch?v=fhfIpUgxgm8&t=91s https://www.youtube.com/watch?v=ee79_7CZ0uM 00:08 https://www.youtube.com/watch?v=7NAKaSo19us 00:05 https://www.youtube.com/watch?v=oMKQPpbIs3Q 01:08	https://iwc.int/lives
Mackerel (kingfish) *Scomberomorus cavalla*	10	1.0	1.83 1.84 1.80	80 90 90	0.11 0.11 0.11	9.1 9.0 8.8	43.9 42.7 40.1	Youtube https://www.youtube.com/watch?v=1HjLZ3k2osI&t=16s 00:11, 00:51 https://www.youtube.com/watch?v=cYQt7Q2ZCUA 00:05 https://www.youtube.com/watch?v=e0_7g6WSLjg https://www.youtube.com/watch?v=9-	Inferred from length-weight curve in FishBase

								pEANtcqW8&t=14s	
Mako shark Genus: *Isurus*	10	2.5	1.67 1.60 1.52	90 90 90	0.10 0.10 0.10	8.2 7.9 7.5	11.3 10.0 8.7	Youtube https://www.youtube.com/watch?v=Qktk9vYRuVc 00:05 https://www.youtube.com/watch?v=F781RwUtFVY 00:26 'Mako jumping' video no longer available on youtube 00:00	FishBase
Mobulid ray[3] Genus: *Mobula*	33	0.7	1.48 1.44 1.40	90 80 90	0.13 0.13 0.13	7.3 7.2 7.0	38.1 36.8 33.9	Youtube https://www.youtube.com/watch?v=EAhCKoVxDZs &t=9s https://www.youtube.com/watch?v=7Lt41sTba_E 00:22, 00:32, 00:54	Chris Lawson, unpublished data
Mullet *Mugil cephalus*	43	0.4	1.20 1.24 1.24	60 90 90	0.14 0.14 0.14	6.1 6.1 5.5	39.8 39.8 29.8	Youtube https://www.youtube.com/watch?v=HuSZo-6RL0o 00:33, 00:37, 00:40	Visual assessment
Orca (Killer whale)† *Orcinus orca*	12	6.5	1.83 1.52 1.33	90 80 90	0.09 0.09 0.09	9.0 7.5 6.5	5.0 2.9 2.0	Youtube https://www.youtube.com/watch?v=lfat0eJMpPA&t= 171s https://www.youtube.com/watch?v=EMVyOMiqTLc https://www.youtube.com/watch?v=aEStursrpiE	Wikipedia

								00:02 https://www.youtube.com/watch?v=W_24PxFbJ6I 00:05 https://www.youtube.com/watch?v=WzhFBx1pwyQ 00:01	
Silver carp[4] *Hypophthalmichthys molitrix*	31	0.8	1.60 1.56 1.56	90 80 90	0.12 0.12 0.12	7.9 7.8 7.7	37.0 35.8 34.5	Youtube https://www.youtube.com/watch?v=x3Bf0WhvsNk 01:22, 02:06, 03:19	Visual assessment, confirmed by FishBase
Spinner dolphin *Stenella longirostris*	12	1.8	2.00 1.03 1.00	80 90 80	0.10 0.11 0.11	10.0 5.2 5.0	28.7 4.3 3.9	Youtube https://www.youtube.com/watch?v=3b4FGlWGsuo 00:31, 01:54 https://www.youtube.com/watch?v=9teNVevwKzU 01:58 https://www.youtube.com/watch?v=B5KNNwO87-8 https://www.youtube.com/watch?v=H70nPv4NQsw	Wikipedia
White shark *Carcharodon carcharias*	12	3.3	1.24 1.16 1.16	80 80 80	0.10 0.10 0.10	6.2 6.0 5.8	3.5 3.2 2.9	The dataset published in (Johnston et al., 2018)	Mean length for individuals in videos, provided by Alison Koch.

[1]Only a single value available.

[2]Breaching velocity values are within the maximum velocity range reported in (Rohr et al., 2002).

[3]Mobulid rays have a very different surface to volume ratio compared to the fusiform (double-ogive) shapes of the other animals represented in the table, and are propelled from mid-body, rather than from the caudal end as other species presented in this study do. Corrections to equations (1) and (2) for mobulid rays can be found in Supplementary Appendix D.

[4]Breaching velocity values very similar to those reported in Parsons et al. (2016)

[5]FishBase

[6]Wikipedia

†Typically, these species did not completely clear the water.

N - Number of breaches included in analyses

l - Estimated standard body length, defined as from distal end to tail fork (m). Some length values taken from sources were for total body length and thus adjusted to approximately account for tail shape.

τ – Breaching duration (s)

γ - Breaching angle of three fastest breaches (°)

A - Ratio of drag coefficient to prismatic coefficient of body; it was estimated using equations (2) and (3) (see also equations (B5) and (B10) of Supplementary Appendix B)

v_0 - Breaching velocity (m/s); it was estimated using equation (1) (see Supplementary Appendix A for details)

P/m – Power to mass ratio (W/kg); it was estimated using equation (5) (see also equation (B12) of Supplementary Appendix B)
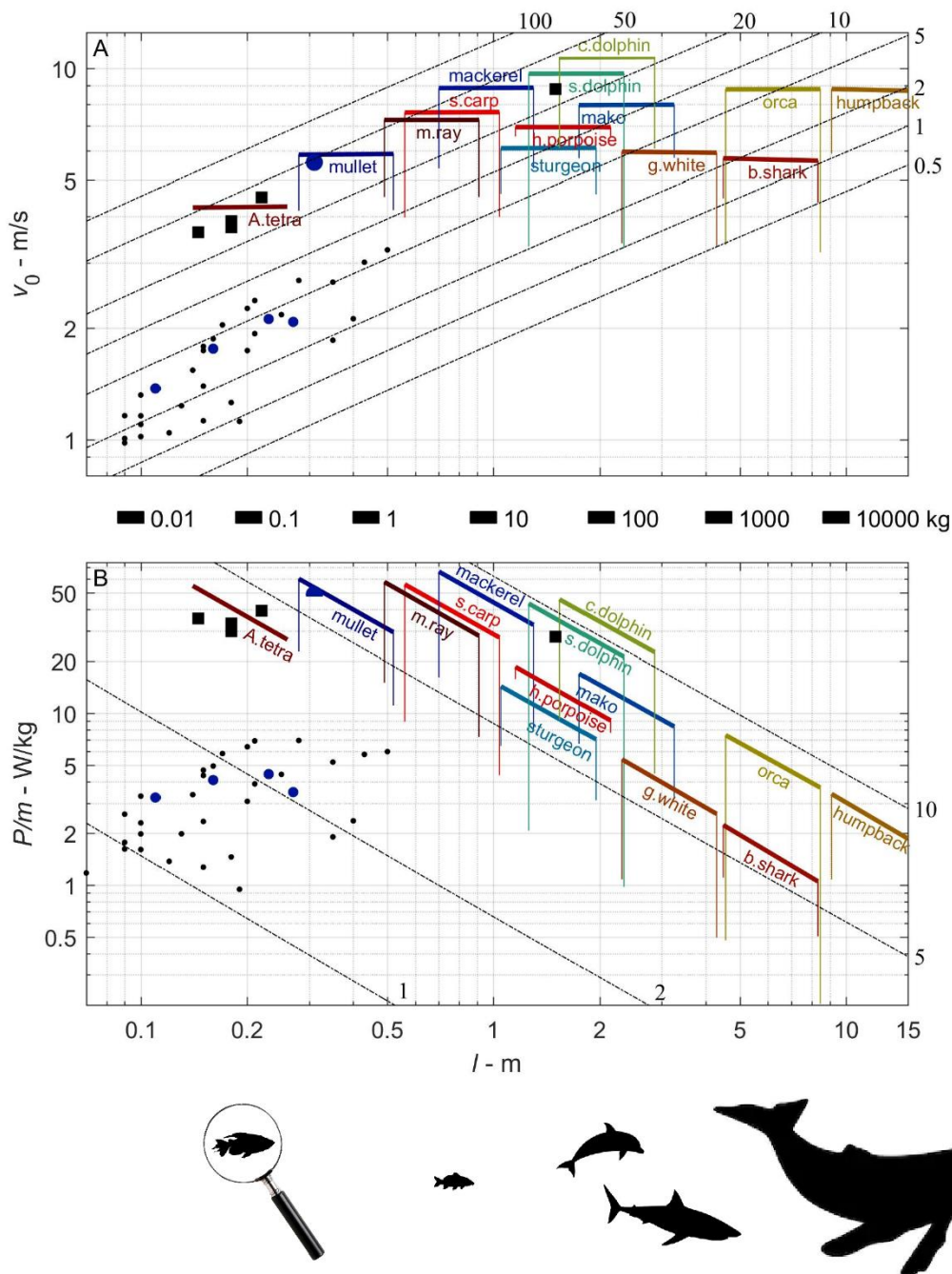
Figures

Figure 1: **The velocity and mechanical power output of breaching animals (n = 14 species) at different body lengths, plotted on logarithmic scales.** A: velocity immediately prior to breaching, v_0 (m/s). The upper boundary of each box represents the maximum velocities observed during breaches for a given species; the left and right boundaries represent the estimated body length of that species with ±30% uncertainty, and they extend down as far as

the minimum breaching velocities observed. Circles mark the burst swimming speed data presented by Videler and Wardle (1991) for multiple fish species; blue are for mackerel, and the larger blue circle represents a single outlier - a swimming speed similar to that exhibited for that size of fish during breaching. Squares mark the maximal speed of trout, herring, barbell and nase swimming in a specialised flume (Castro-Santos et al., 2012; Sanz-Ronda et al., 2015), and sailfish hunting at sea (Marras et al., 2015). The dash-dot lines mark constant mechanical power-to-mass ratios (in W/kg; magnitudes indicated). B: The same data and formatting as A, however the ordinate represents mass-specific power, and the dash-dot lines mark constant speed (in m/s, magnitudes indicated). The silhouettes are four breaching species to scale (silver carp, common dolphin, white shark, humpback whale) and also the African tetra, magnified 6 fold. Across species, body length relates only very approximately with body mass, however to provide some idea of how breaching velocity and mass-specific power scale with body mass, the black boxes between the figures denote the possible range of lengths of aquatic animals (associated with different body proportions) that have the mass (kg) indicated to the right of the box. A. tetra: African tetra; m. ray: mobulid ray; s. carp: silver carp; h. porpoise: harbour porpoise; s. dolphin: spinner dolphin; c. dolphin: common bottlenose dolphin; g. white: great white shark; b. shark: basking shark.
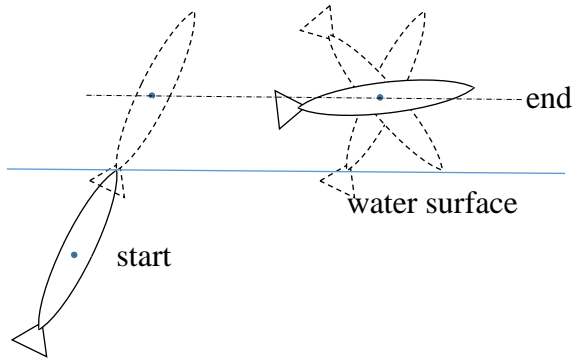
Figure A1: The start and end of a jump. The frame count starts when the nose pierces the water; the count ends when the centre of mass returns to the same height above the water as it were when the tail cleared the water on the way up.
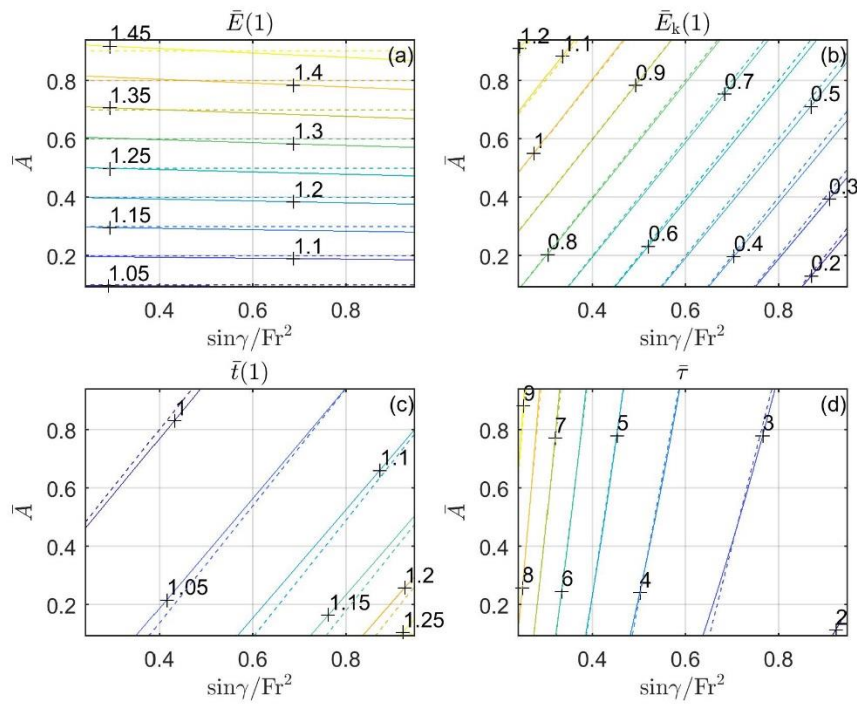

Figure A2: Approximate (dashed) versus exact quantities. Contours of total energy ((A31) and (A53)) are shown on (a); contours of the kinetic energy ((A34) and (A52)) are shown on (b); contours of the crossing time ((A35) and (A54)) are shown on (c); contours of the air time (the conjunction of (A36) and (A35) versus (A56)) are shown on (d).
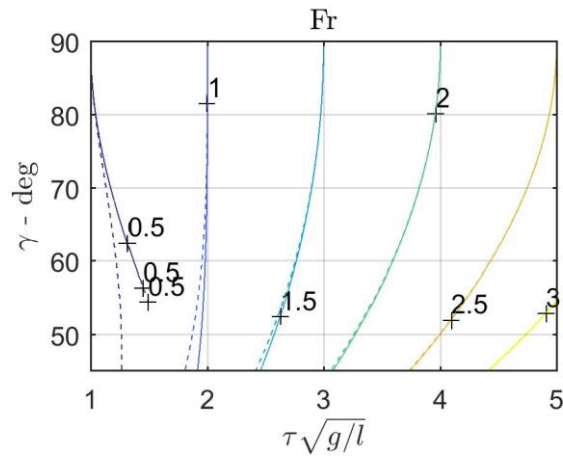
Figure A3: Estimating the Froude number from air time. The figure is based on solutions of (A56)-(A59) with $\bar{A} = 0$. The approximate solution (A61) is dashed; the exact solution (A60) is marked solid. The accuracy suffers when the breaching angle is less than about 70°.
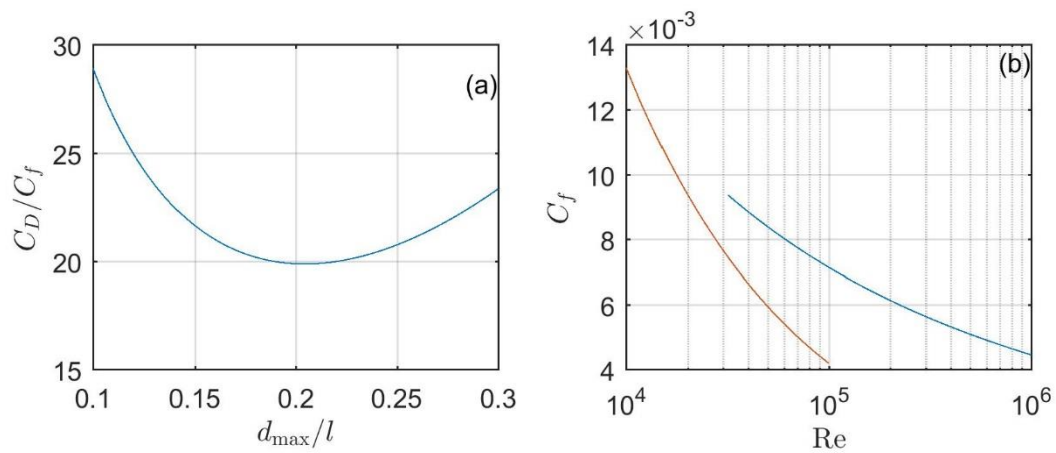

Figure B1: The coefficient with C_f in equation (B8) (a) and C_f (b). Most fish have d_{max}/l in the range (0.15, 0.25), and hence the coefficient in equation (B8) can be closely approximated by 20. The right curve on (b) represents a turbulent boundary layer (B5); the left curve represents the laminar one (B6).
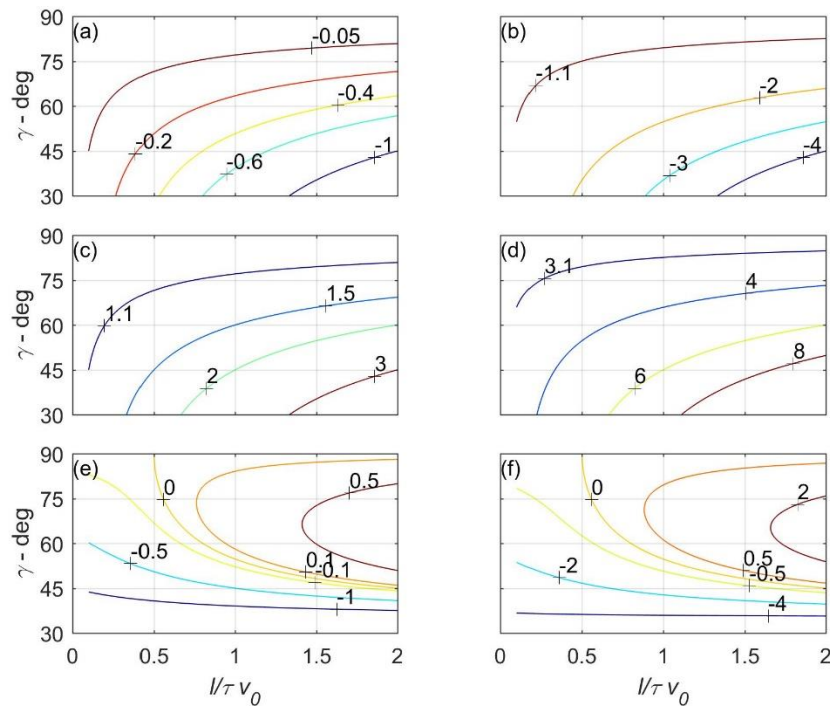
Figure C1: The left column shows contour maps of the derivatives $\dfrac{\partial \ln v_0}{\partial \ln l}$, $\dfrac{\partial \ln v_0}{\partial \ln \tau}$, and $\dfrac{\partial \ln v_0}{\partial \bar{\gamma}(1)}$ (plates a, c, e); the right column shows the derivatives $\dfrac{\partial \ln (P/m)}{d \ln l}$, $\dfrac{\partial \ln (P/m)}{d \ln \tau}$, and $\dfrac{\partial \ln (P/m)}{d \bar{\gamma}(1)}$ (plates b, d, f).
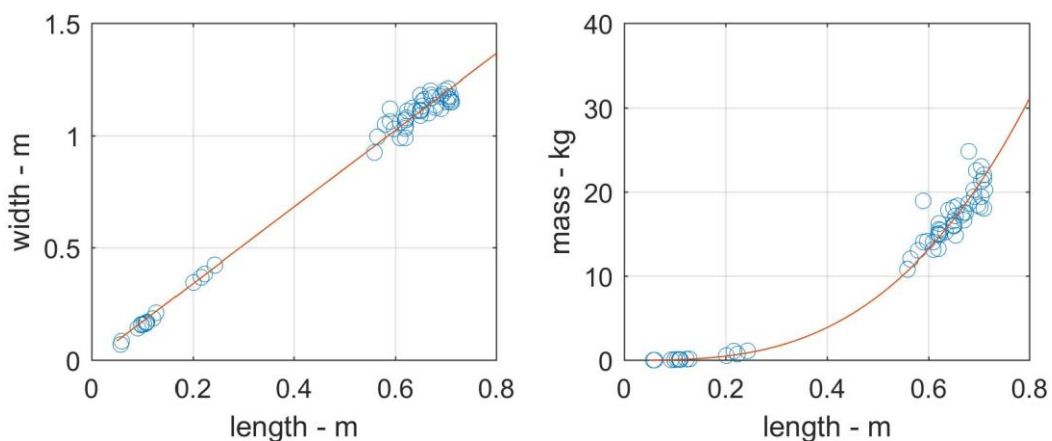

Figure D1: Width-length and mass-length relations for mobulid rays. The red lines are regressions $w = \bar{w}l$ and $m = \rho\bar{m}l^3$ with $\bar{w} = 1.7$ and $\bar{m} = 0.06$. Based on data courtesy of Chris Lawson.